ACS APPLIED MATERIALS & INTERFACES

Research Article

www.acsami.org

Simple Preparation of Carbon Nanofibers with Graphene Layers Perpendicular to the Length Direction and the Excellent Li-Ion Storage Performance

Tao Li,[†] Cheng Wei,[†] Yi-Min Wu,[†] Fu-Dong Han,[†] Yong-Xin Qi,[†] Hui-Ling Zhu,[‡] Ning Lun,*[,†] and Yu-Jun Bai*[,†]

[†]Key Laboratory for Liquid−Solid Structural Evolution and Processing of Materials (Ministry of Education), Shandong University, Jinan 250061, People's Republic of China

[‡]School of Materials Science and Engineering, Shandong University of Science and Technology, Qingdao 266590, People's Republic of China

Supporting Information

ABSTRACT: Sulfur-containing carbon nanofibers with the graphene layers approximately vertical to the fiber axis were prepared by a simple reaction between thiophene and sulfur at 550 °C in stainless steel autoclaves without using any templates. The formation mechanism was discussed briefly, and the potential application as anode material for lithium-ion batteries was tentatively investigated. The carbon nanofibers exhibit a stable reversible capacity of 676.8 mAh/g after cycling 50 times at 0.1 C, as well as the capacities of 623.5, 463.2, and 365.8 mAh/g at 0.1, 0.5, and 1.0 C, respectively. The excellent electrochemical performance could be attributed to the effect of sulfur. On one hand, sulfur could improve the reversible capacity of carbon materials due to its high theoretical capacity; on the other hand, sulfur could promote the formation of the unique carbon nanofibers with the graphene layers perpendicular to the axis direction, favorable to shortening the Li-ion diffusion path.

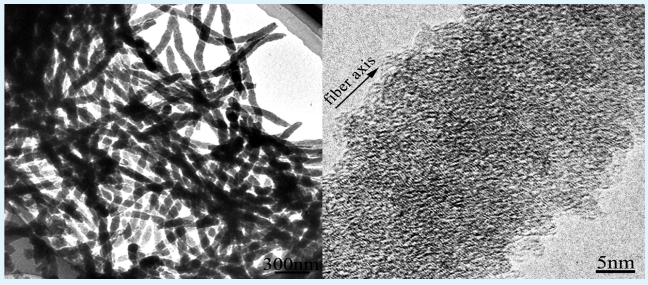

KEYWORDS: *carbon nanofiber, electrochemical performance, anode material, rate capability*

1. INTRODUCTION

The combination of low cost and abundance with good electronic conductivity, low charge/discharge potential, high safety, and cycling stability enables graphite to be the dominant anode material for the present-day commercial Li-ion batteries (LIBs). The graphene sheets in graphite are bonded together by van der Waals forces, allowing the intercalation/deintercalation reaction of Li ions ($6C + Li^+ + e^- \leftrightarrow LiC_6$) between them to yield a theoretical specific capacity of 372 mAh/g. The low capacity and the poor rate performance of graphite cannot meet the ever-increasing demand for high energy density and high power density. Thus, a lot of investigations have been focused on exploring alternative carbon materials to substitute for graphite as the anode materials.[1−6] In general, the graphene layers of one-dimensional (1D) carbon materials, such as carbon fibers and tubes, are parallel to the length direction; that is, the *c*-axis is perpendicular to the fiber or tube axis. Long carbon nanotubes as the anode materials for LIBs could not exhibit good electrochemical performance because of the long diffusion distance of Li ions between the graphene layers to fully lithiate the nanotubes.[5,7] However, the electrochemical performance could be improved by forming short carbon nanotubes.[7−9] Enlightened by the enhanced electrochemical performance resulting from shortening the length of carbon nanotubes, changing the array mode of graphene layers in 1D carbon materials might improve the Li-ion storage performance; however, there is no evidence for this to date.

Recently, carbon nanofibers and nanotubes with the graphene layers nearly vertical to the axis direction have attracted some interest. Although the mechanical strength and electrical and thermal conductivities of the carbon nanofibers with the graphene layers perpendicular to the length direction are generally inferior to those of the common nanofibers with the graphene layers parallel to the axis direction, they could reveal a variety of potential applications as chemical sensors, gas adsorbents, energy-storage batteries, and supercapacitors due to the high density of active sites on their surfaces.[10−12] Laude et al. prepared carbon fibers with the graphene layers nearly perpendicular to the fiber axis by decomposing acetylene in the presence of $FeCl_2$ vapors via chemical vapor deposition (CVD).[13] Hurt et al. synthesized carbon nanofibers with the graphene layers orthogonal to the fiber axis by template-mediated assembly of discotic mesophase pitch using alumina

Received: August 19, 2014
Accepted: February 23, 2015
Published: February 23, 2015

DOI: 10.1021/am508862e
ACS Appl. Mater. Interfaces 2015, 7, 5107−5115

nanochannel arrays as three-dimensional edge-on surface anchoring templates.[10] Konno et al. fabricated platelet structure carbon nanofilaments by liquid phase carbonizing polymer powders in Al-based porous templates.[14] Müllen et al. prepared carbon nanotubes with controllable graphene-layer orientation using anodic alumina membranes with open and separated straight channels as templates.[15] Li et al. fabricated carbon nanopods with the graphene layer orientation perpendicular/parallel to their long axis by simply changing synthesis conditions.[16] However, from the literature available, the preparation of carbon fibers with the graphene layers perpendicular to the fiber axis needs complex synthesis conditions and is thus unfavorable for economical production in large-scale. As a consequence, simply and economically synthesizing the 1D carbon materials with the graphene layers perpendicular to the axis direction is still a great challenge.

Sulfur has been reported to play a key role in synthesizing carbon nanostructures. As early as 1981, Katsuki et al. reported that sulfur exerted an importantly catalytic effect to produce carbon fibers.[17] In the subsequent years, the role of sulfur in synthesizing vapor-grown carbon fibers from pyrolyzing hydrocarbon with different metallic catalysts in the presence of sulfur additives (e.g., thiophene or hydrogen sulfide) was further studied. Kim et al. found that low sulfur coverage on cobalt catalyst changed the catalytic activity due to charge rearrangement in neighboring atoms, thus favoring C−C bond rupture in the absorbed molecules, which subsequently precipitated into carbon filaments.[18] Tibbetts et al. observed that iron particles did not grow filaments in a methane atmosphere, but adding small quantities of sulfur to the iron vastly increased the filament formation.[19] The increased catalytic activity of Fe by introducing sulfur favored the fiber formation in a vapor−liquid−solid growth mode.[19] Ci et al. reported that only an optimal amount of sulfur addition was needed to obtain filamentous carbon.[20] Romo-Herrera et al. obtained different types of nanostructures with various amounts of sulfur inside the carbon material using ferrocene and nickelocene as catalyst and sulfur-containing additive (thiophene) as carbon feedstock, where sulfur not only acted as the catalyst but also diffused and incorporated into the sp^2 carbon lattice of the nanostructure to induce curvature.[21] Thus, it can be seen that sulfur could play an important role in synthesizing the carbon fibers.

In this work, we prepared sulfur-containing carbon nanofibers with the graphene layers nearly vertical to the length direction by the simple reaction between thiophene and sulfur at 550 °C in stainless steel autoclaves without using any templates. Though the formation mechanism is presently not yet understood clearly, a brief discussion was presented according to the experimental results. By tentatively using the sulfur-containing carbon nanofibers with the unique structural feature as anode materials for LIBs, a high reversible capacity of 676.8 mAh/g is retained after cycling 50 times at 0.1 C, and excellent rate performance could be achieved at 0.1−1.0 C.

2. EXPERIMENTAL SECTION

2.1. Material Preparation. Chemically pure thiophene and sulfur were used as raw materials. In a typical procedure to prepare carbon nanofibers, 4.0 mL of thiophene and 9.6 g of sulfur (corresponding to a molar ratio of 1:6) were added into a stainless steel autoclave of 30 mL in capacity. As a reactor, the tightly sealed autoclave was heated at 550 °C for 5 h, followed by naturally cooling to ambient temperature. The powder product collected from the bottom of autoclave was first washed with boiling CCl_4 (boiling point: 76.8 °C) to remove the residual sulfur and was then rinsed successively with absolute ethyl alcohol and deionized water. The resulting dark product dried at 50 °C for 12 h is 2.49 g in weight, and is designated as S6. For comparison, another two experiments were conducted also at 550 °C for 5 h, and the product derived from the direct pyrolysis of 4.0 mL of thiophene is denoted as S0, and that from the reaction of 4.0 mL of thiophene and 3.2 g of sulfur (corresponding to a molar ratio of 1:2) as S2.

2.2. Characterization. A Rigaku Dmax-rc diffractometer with Ni-filtered Cu Kα radiation (V = 50 kV, I = 80 mA) was adopted to collect X-ray diffraction (XRD) patterns at a scanning rate of 4°/min. The morphology was examined by a Hitachi SU-70 field emission scanning electron microscope (FESEM) equipped with an energy-dispersive X-ray spectrometer (EDX) and by a JEOL JEM-2100 high-resolution transmission electron microscope (HRTEM). Nitrogen adsorption/desorption isotherms were acquired at −196 °C in a Quadrasorb SI sorption analyzer with the samples being degassed at 300 °C for 3 h under a vacuum in the degas port. The Brunauer−Emmett−Teller (BET) model was used to calculate specific surface area. The composition of the products was recorded on a KARTOS XSAM800 X-ray photoelectron spectrometer (XPS), using Al Kα ($h\nu$ = 1486.6 eV) radiation as the excitation source with an anode voltage of 12 kV and an emission current of 10 mA. Furthermore, Raman spectra of the products were acquired using a Lab-RAM HR800 Raman spectrometer, and the element content was determined by a Vario EL III elemental analyzer.

2.3. Electrochemical Measurements. CR2025 coin-type half-cells were used for electrochemical evaluation. The working electrodes were fabricated by mixing the samples, acetylene black, and polyvinylidene fluoride (PVDF) dissolved in *N*-methyl-2-pyrrolidinone (NMP) with a weight ratio of 80:10:10. The uniformly mixed slurry was coated onto a copper foil and dried at 120 °C in vacuum for 12 h. Metal Li foils were used as counter electrode, Celgard 2300 as separator, and a mixture of 1 M $LiPF_6$ solved in ethylene carbonate (EC) and dimethyl carbonate (DMC) (1:1 by volume) as electrolyte. The assembly of half-cells was carried out in an argon-filled glovebox at ambient temperature. Galvanostatic charge−discharge was performed on a LAND CT2001A battery test system at various current densities in the voltage range of 0.02 and 3.0 V versus Li^+/Li at room temperature. For convenience of comparison, the current density was set using the specific capacity of graphite (372 mAh/g) as a basis. The actual weight of active materials in each electrode is ∼3.0 mg. Cyclic voltammograms (CV) were acquired on an IviumStat electrochemical workstation between 0.01 and 3.0 V with a scan rate of 0.3 mV s^{-1}, and electrochemical impedance spectra (EIS) were tested with an alternating current signal amplitude of 5 mV in the frequency range from 100 kHz to 0.1 Hz.

3. RESULTS AND DISCUSSION

3.1. Structure, Morphology, and Composition. The XRD patterns of the products obtained by the reaction of thiophene with various sulfur contents are shown in Figure 1. The widened diffraction peaks around 2θ = 25 and 43° resulted from the (002) and (100) plane of carbon material suggest the low graphitization degree. No obvious characteristic peaks associated with sulfur could be distinguished from the XRD patterns, indicating that there is no crystalline sulfur in the products. Furthermore, the peak width of (002) peak decreases, and the peak position shifts slightly to a higher angle with increasing the sulfur content in the reactants, demonstrating the decreased spacing of (002) plane and increased graphitization degree, because sulfur could improve the dehydrogenation from thiophene,[17] as evidenced by the following elemental analysis. Note that the (100) peak of S0 is slightly stronger than that of S2 and S6 owing to the higher carbon content in S0 than in S2 and S6. The carbon materials with low graphitization degree and larger interlayer spacing (compared with graphite) is

DOI: 10.1021/am508862e
ACS Appl. Mater. Interfaces 2015, 7, 5107−5115

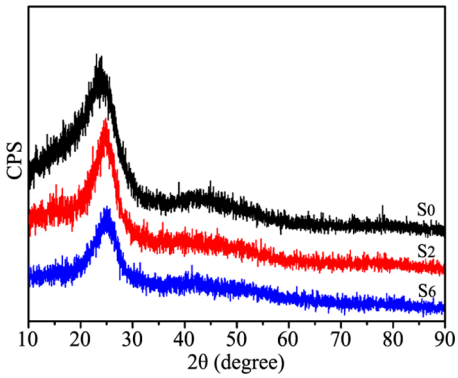

Figure 1. XRD patterns of S0, S2, and S6.

favorable for the Li-ion insertion/extraction between the graphene layers.[6,22]

The FESEM images of the products are displayed in Figure 2, from which the morphology changes significantly with the varying sulfur content added in the reactants. When no other sulfur was added, the pyrolysis product of thiophene is composed of microspheres with smooth surface and diameter of 4−8 μm (Figure 2a). Composition analysis verifies the uniform coexistence of carbon and sulfur in the microspheres (Figure S1 in Supporting Information). In the product of S2, besides the formation of microspheres, some short nanofibers were also inspected (Figure 2b), which are either on the surface of the microspheres or assembled into clusters like cotton wool. Furthermore, in the product of S6, a large number of nanofibers with few microspheres were observable (Figure 2c). From the corresponding elemental mappings in Figure 2d,e, carbon and sulfur distribute homogeneously across the whole sample in the nanofibers. The EDX spectrum displayed in Figure 2f further confirms the presence of carbon and sulfur in the nanofibers. The nanofibers in S2 and S6 are clear under TEM, as revealed in Figure 3. The short nanofibers in S2 are ∼40 nm in diameter and 200−600 nm in length (Figure 3a,b), while the nanofibers in S6 (Figure 3c) are tens of micrometers in length, yet with the similar diameter to those in S2, demonstrating that the nanofibers grow along the length direction rather than along the radial direction. Despite the difference in length, the lattice fringe images of the nanofibers are analogous to each other, as exemplified by the HRTEM image in Figure 3d. An apparent feature of the nanofibers is that the graphene layers are almost perpendicular to the length direction, significantly dissimilar to those observed in the common carbon fibers and tubes where the (002) plane is parallel to the axis direction. Another feature is that the graphene layers are intermittent accompanying the presence of some amorphous phases in the nanofibers, resulting in the low graphitization degree and rugged surfaces. These unique structures could provide more free space and shortened distance for Li-ion diffusion compared to the common carbon fibers and tubes and thus could be beneficial for the reversible Li-ion storage when used as anode materials for LIBs.[11] The morphology change from microsphere to nanofiber could give rise to the increase in surface area. As calculated from the nitrogen adsorption/desorption isotherms using BET model, the specific surface area is 10.8 $m^2\ g^{-1}$ for S0, 12.3 $m^2\ g^{-1}$ for S2, and 107.5 $m^2\ g^{-1}$ for S6. The large surface area of S6 could provide sufficient contact between electrode materials and electrolyte, beneficial for fast Li-ion transfer and enhancing the electrochemical performance.

To determine the binding of carbon with sulfur, XPS measurement was carried out, as shown in Figure 4. From the survey spectra in Figure 4a, the dominant elements in the three products are carbon, sulfur, and oxygen. The oxygen could be ascribed to the air absorbed on the products. It is apparent, with the increasing content of sulfur in the reactants, the intensity of S 2p signal increases. The high-resolution spectra of C 1s (Figure 4b) could be deconvoluted into three peaks; the ones located at 284.6 and 285.6 eV correspond to C═C and C−C carbon interactions, respectively, and the one at 286.5 eV corresponds to C−S bonding,[23−25] demonstrating the strong interaction between carbon and sulfur. Moreover, in the high-

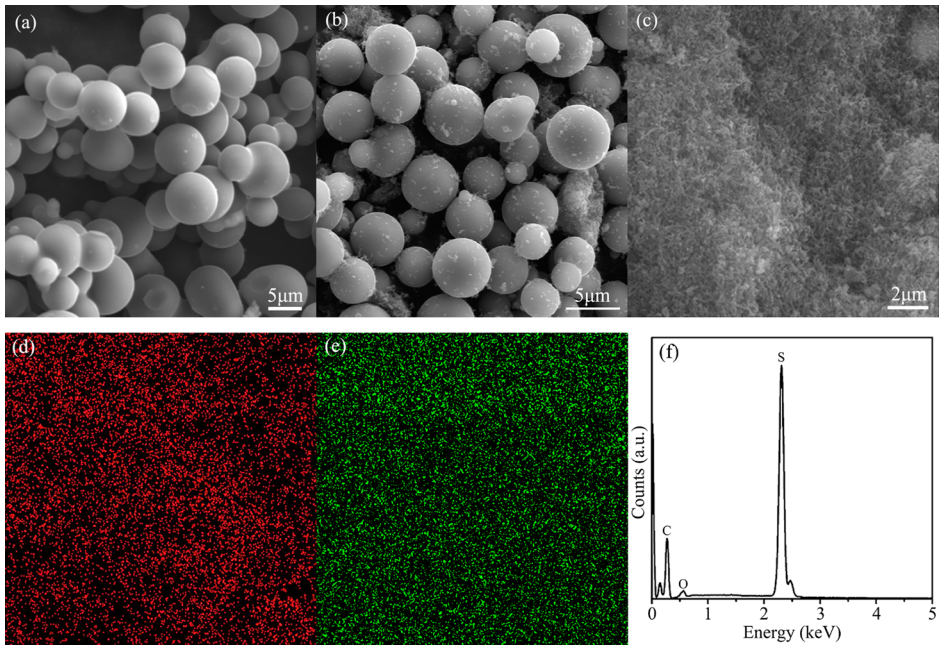

Figure 2. FESEM images of S0 (a), S2 (b), S6 (c). For S6, the elemental mappings of carbon (d), sulfur (e), and EDX spectrum (f).

DOI: 10.1021/am508862e
ACS Appl. Mater. Interfaces 2015, 7, 5107−5115

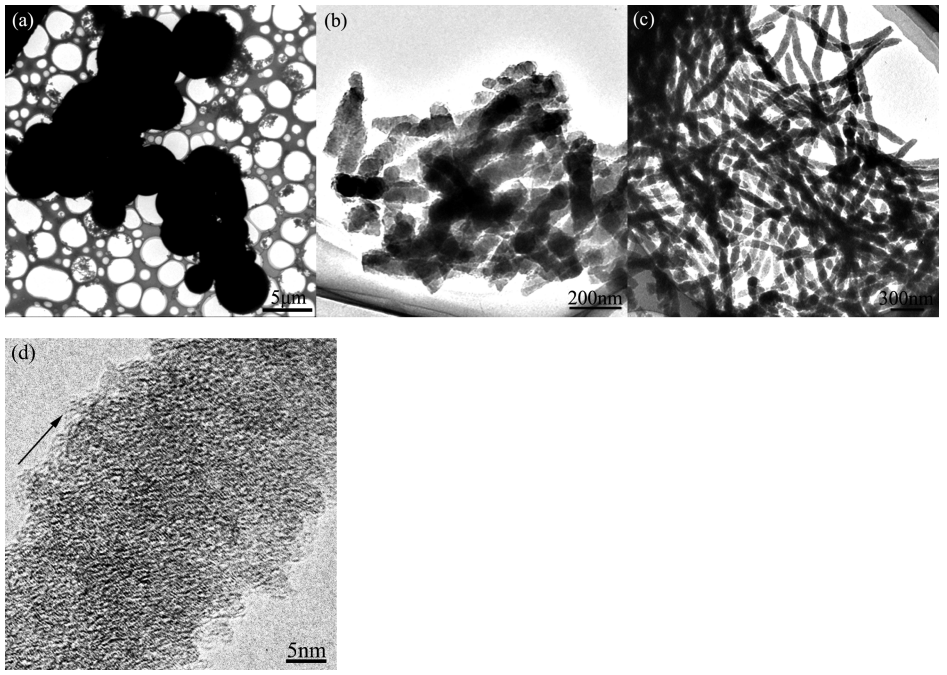

Figure 3. TEM images of S2 (a, b), S6 (c), and the lattice fringe image of the nanofibers (d). The arrow in (d) indicates the fiber axis.

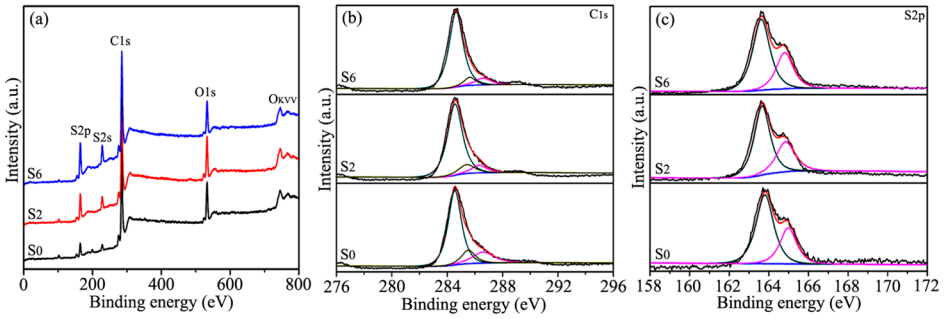

Figure 4. XPS spectra of S0, S2, and S6. (a) Survey spectra, (b) C 1s spectra, and (c) S 2p spectra.

resolution spectra of S 2p (Figure 4c), the two peaks around 163.7 and 165.1 eV are ascribed to the sulfur bonded in cyclic carbon structure. The binding energies are slightly higher than those that resulted from elemental sulfur, indicating that the signals originate from the chemically bonded sulfur.[24,26−29] Sample S0 derived from the direct pyrolysis of thiophene, so sulfur exists in the form of C−S bonds, while samples S2 and S6 derived from the reaction of thiophene and sulfur; besides the sulfur in thiophene-like structure, some sulfur added might produce strong interaction with the carbon yielded to form C−S bonds, and this part of sulfur could not be removed even after washing thoroughly with boiling CCl_4. Furthermore, the similarities in peak appearance and position for both C 1s and S 2p also demonstrate the consistency of the bonding between carbon and sulfur in the three samples despite the varied peak intensities owing to the difference in sulfur content. The presence of C−S bonds could also be confirmed by thermogravimetric analysis (TGA) under nitrogen flow, as shown in Figure S2 of the Supporting Information. (Owing to the limitation of TGA apparatus, the curve was measured only from ambient temperature to 800 °C, and part of sulfur is still in the carbon materials due to the incomplete C−S bond fission.) From Figure S2, the weight loss of S0 only occurs above 600 °C due to the fission of C−S bond in thiophene-like structure, while the weight loss of S6 begin from ∼250 °C persistently to 800 °C with an inflection at ∼600 °C. The weight-loss curves are markedly different from those presented in the C/S composites,[30−32] where the weight loss begins and finishes within a narrow temperature range at ∼250 °C. The successive weight loss between 250 and 800 °C in S6 demonstrates that the sulfur in the carbon nanofibers does not simply composite with carbon but form C−S bonds.[32] Because of the difference between the C−S bonds resulting from the interaction of the sulfur added with the carbon yielded and those in the thiophene-like structure, different stabilities occur during heating. Some of the former ones rupture first in the temperature range of 250−600 °C due to the weak bonding, and the residues break above 600 °C with the latter ones owing to the strong interaction, resulting in the two stages of weight loss in the TGA curve shown in Figure S2.

Elemental analysis was also performed to evaluate the element content in the products. The results are summarized in Table S1 of Supporting Information. The weight percent of sulfur is 23.0 wt % for S0, 35.6 wt % for S2, and 42.9 wt % for S6. Apparently, the sulfur content in the product increases with the increasing amount added in the reactants, in accordance with the XPS result. Moreover, the decreased hydrogen content and increased C/H ratio with the increasing amount of sulfur

DOI: 10.1021/am508862e
ACS Appl. Mater. Interfaces 2015, 7, 5107−5115

demonstrate the enhanced dehydrogenation resulting from sulfur, as discussed in the XRD analysis.

Raman spectroscopy was acquired to verify the structure of the products. From the spectra in Figure 5, besides the D-band

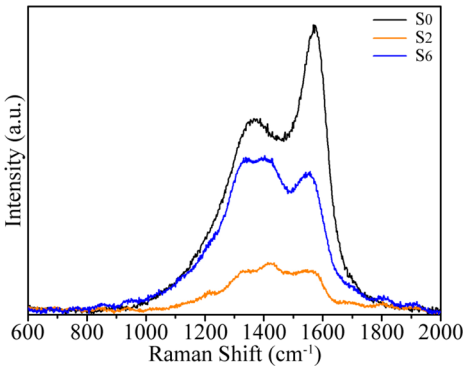

Figure 5. Raman spectra of S0, S2, and S6.

around 1329 cm^{-1} resulting from the disordered carbon structure and the G-band around 1571 cm^{-1} from the crystalline graphite,[25,33,34] another two peaks around 1230 and 1408 cm^{-1} might be associated with the different C−S bonds by combining the XPS result in Figure 4 and the TGA result in Figure S2 with the Raman results in the literature.[35,36] The ratio of integral intensity for G peak to D peak (I_G/I_D) could reflect the crystallization degree of carbon materials.[2,37] The relatively low I_G/I_D ratio demonstrates the low graphitization degree of the carbon microspheres and nanofibers, consistent with the XRD and TEM results stated above.

3.2. Formation Mechanism for the Carbon Nanofibers. Though an unambiguous formation mechanism for the carbon nanofibers with the graphene layers perpendicular to the length direction is not well-understood currently, a series of experimental results could confirm the critical role of sulfur in synthesizing the carbon nanofibers. Without the addition of sulfur (S0), the direct pyrolysis of thiophene at 550 °C could only result in the formation of carbon microspheres (Figure 2a). In the reaction between thiophene and sulfur with a molar ratio of 1:2 (S2), only a small quantity of short carbon nanofibers formed with their graphene layers perpendicular to the axis direction (Figures 2b and 3a,b). However, when the molar ratio of thiophene to sulfur reaches 1:6 (S6), large quantities of long carbon nanofibers could be obtained with their graphene layers approximately vertical to the axis direction (Figures 2c and 3c), demonstrating the promotion of sulfur on the morphology change from microsphere to nanofiber. From the experimental results, without the participation of sulfur, thiophene thermally homopolymerizes into polythiophene microspheres first and then pyrolyzes into carbon microspheres at 550 °C. In the presence of sulfur, the molten sulfur could uniformly mix with thiophene in liquid state when the temperature is above 106.8 °C (melting point of sulfur), suppressing the homopolymerization of thiophene to some degree with varied molar ratios of thiophene to sulfur. At a molar ratio of 1:2 (S2), the homopolymerization of thiophene could only be inhibited partially, and the interaction of sulfur with thiophene changed the polymerization mode of a small amount of thiophene, resulting in the formation of a small quantity of short carbon nanofibers with the graphene layers perpendicular to the axis direction during pyrolysis. However, most of the thiophene could still polymerize into polythiophene microspheres followed by pyrolyzing into carbon microspheres at 550 °C. When the molar ratio increases to 1:6 (S6), the homopolymerization of thiophene could be almost completely suppressed, leading to the formation of large quantities of long carbon nanofibers with the graphene layers nearly perpendicular to the length direction. As a further confirmation of the role of sulfur, we carried out another three experiments in which *n*-heptane was used to substitute for thiophene to react with sulfur under the similar conditions. The molar ratio of *n*-heptane to sulfur is 1:0, 1:4, and 1:16, and the corresponding products are assigned to A0, A4, and A16. From the TEM images (Figure S3 in Supporting Information), with the increasing sulfur content from 1:0 to 1:16, the morphology of the product changes also from microsphere to nanofiber, just like what happened in the reaction between thiophene and sulfur, indicative of the important role of sulfur in achieving the carbon nanofibers. Although no catalyst was deliberately added in the experiments, the stainless steel autoclave itself could act as the catalyst for forming carbon nanofibers. When the thiophene and sulfur with a molar ratio of 1:6 were put in a quartz tube placed in an autoclave and heated at 550 °C for 5 h, there are no carbon nanofibers in the product collected from the tube, though the morphology of the product changes from microsphere to porous carbon materials (Figure S4 in Supporting Information). Thus, it can be seen, the stainless steel is the catalyst during synthesizing the carbon nanofibers, and sulfur acts as the promoter to change the morphology and arrangement of the graphene layers, just like what has been reported in the literature;[18−21] that is, the formation of carbon nanofibers could be attributed to the promotion of sulfur on the morphology change under the catalysis of stainless steel.

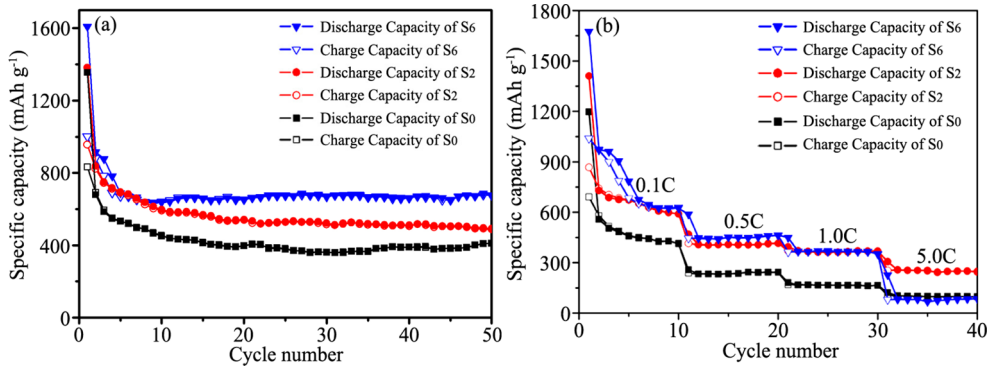

Figure 6. Cycling performance at 0.1 C (a), and rate capabilities at 0.1, 0.5, 1.0, and 5.0 C for every 10 cycles (b) of S0, S2, and S6.

DOI: 10.1021/am508862e
ACS Appl. Mater. Interfaces 2015, 7, 5107−5115

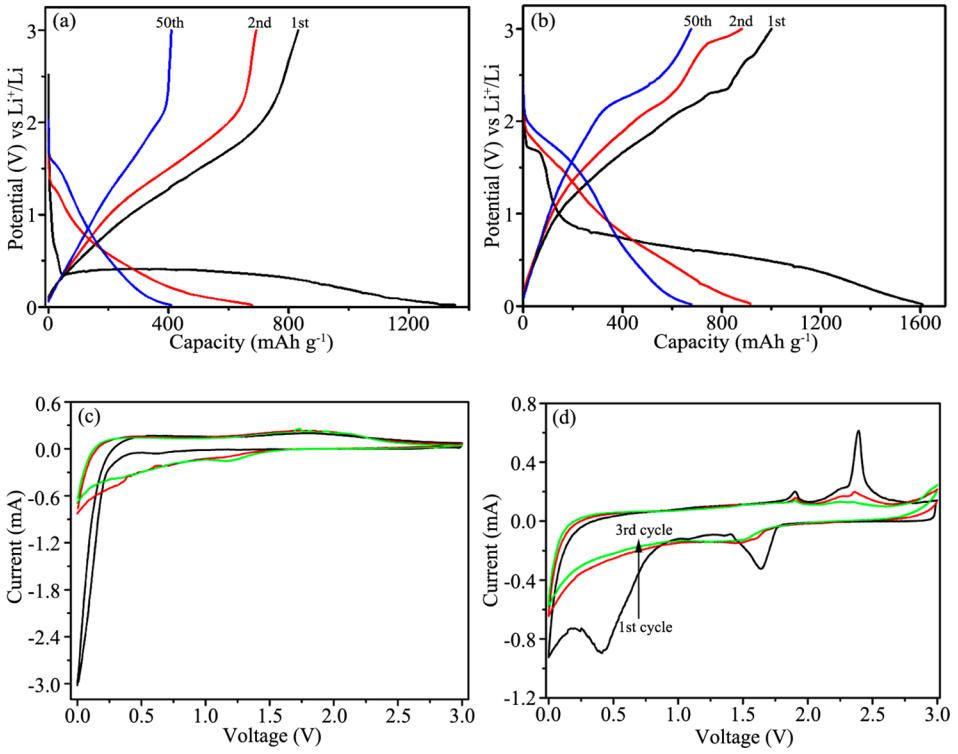

Figure 7. Galvanostatic charge−discharge curves for selected cycles tested at 0.1 C and CV profiles at a scanning rate of 0.3 mV s^{-1} of S0 (a, c) and S6 (b, d).

Besides being the promoter to dehydrogenate from thiophene,[17] sulfur could also increase the activity of metal catalysts[18,19] and incorporate into sp^2 carbon lattice,[21] which is favorable for the formation of sulfur-containing carbon nanofibers. However, the detailed formation mechanism of the nanofibers needs further investigation.

3.3. Electrochemical Performance. In the sulfur-containing carbon nanofibers, the graphene layers perpendicular to the length direction intermittently accompany the presence of some amorphous phases in the fibers. The unique feature is reminiscent of the unusual electrochemical performance of the nanofibers as the anode materials for LIBs. The specific capacities are calculated based on the carbon and sulfur in the products. From the cycling performance revealed in Figure 6a, the three samples exhibit high initial capacities (1354.1 mAh/g for S0, 1382.6 mAh/g for S2, and 1608.2 mAh/g for S6) when measured galvanostatically at 0.1 C, which decay rapidly during the first several cycles. From the fifth cycle, S6 reaches a stable reversible capacity of 687.1 mAh/g, and after 50 cycles the capacity is 676.8 mAh/g with a Coulombic efficiency close to 100%. For S0 and S2, although the Coulombic efficiency is also close to 100% after five cycles, the capacities after the 50th cycle are 408.4 and 490.7 mAh/g, respectively, lower than that for S6, demonstrating that the reversible capacity increases with the increasing sulfur content in the carbon materials, because sulfur could deliver a higher theoretical capacity (1675 mAh/g) than carbon.

The rate capabilities were tested at 0.1, 0.5, 1.0, and 5.0 C for every 10 cycles, as shown in Figure 6b. At the corresponding rates, the capacities are 412.4, 241.9, 165.2, and 96.1 mAh/g for S0, 589.2, 414.7, 368.7, and 243.9 mAh/g for S2, and 623.5, 463.2, 365.8, and 88.9 mAh/g for S6. Obviously, when the rate is no more than 1.0 C, the samples containing the carbon nanofibers (S2 and S6) exhibit higher rate performance, demonstrating the significant role of the carbon nanofibers with the graphene layers nearly vertical to the length direction in Li-ion storage. However, at 5.0 C, the reversible capacity of S6 is lower than that of S2, because the excess sulfur content could give rise to the decrease in electronic conductivity of carbon materials.[38−41] For comparison, the electrochemical performance of the common carbon nanotubes with the graphene layers parallel to the length direction (purchased from Shenzhen Nanotech Port Co. Ltd., China, 20−40 nm in outer diameter and 5−15 μm in length as revealed in TEM images in Figure S5 of Supporting Information) was also tested (Figure S6 in Supporting Information). The nanotubes exhibit inferior cycling stability and rate capabilities under the same test conditions as those of the sulfur-containing carbon nanofibers with the graphene layers nearly vertical to the length direction. The reversible capacity of S6 is ∼3 times of that of the commercial carbon nanotubes with the graphene layers parallel to the length direction tested at the same rates (0.1−1.0 C), implying the potential application of the sulfur-containing carbon nanofibers as anode materials for Li-ion storage.

To know about the stability of the sulfur-containing carbon nanofibers during cycling, the cells of S6 after cycling 50 times were dissected, and the electrode materials were washed thoroughly with acetone and ethanol. From the TEM images (Figure S7 in Supporting Information), the nanofibers retain the 1D morphology, indicative of the good stability of the nanofibers during charging/discharging. The stable morphology could ensure the superior cycling performance of the nanofibers as anode materials for LIBs.

From the above results, the sulfur-containing carbon nanofibers (S6) could be a promising candidate as anode materials for high-performance LIBs. The electrochemical performance (including the cycling stability, rate performance, and reversible capacity) of the carbon nanofibers synthesized in

DOI: 10.1021/am508862e
ACS Appl. Mater. Interfaces 2015, 7, 5107−5115

this work is superior to other carbonaceous materials ever reported, especially carbon nanotubes,[5,7,42,43] electrospun carbon nanofibers,[44−46] and graphene.[47,48] The enhanced performance could be ascribed to the unique sulfur-containing 1D structure with the intermittent graphene layers vertical to the axis direction,[11,49] ensuring the shortened diffusion path and rapid intercalation/extraction of Li ions.

As discussed above, sulfur plays an important role in the formation the nanofibers with the unique feature and in improving the electrochemical performance. On one hand, the participation of sulfur in the reaction changes the morphology of carbon materials from microsphere to nanofiber with the graphene layers nearly perpendicular to the axis direction. On the other hand, the sulfur-containing nanofibers with the unique feature are favorable for not only the increase in the reversible capacity due to the high theoretical capacity of sulfur but also the significant enhancement in the rate capability owing to the shortened diffusion path in the carbon nanofibers with the graphene layers vertical to the length direction. In a word, the performance is associated greatly with the morphology change resulting from the introduction of sulfur, that is, the improved performance of S6 is due to the effect of sulfur in essence. However, too much sulfur in the nanofibers will result in the poor rate performance at high current rates owing to the decreased electronic conductivity, as evidenced by the following EIS.

For a better understanding of the electrochemical reaction mechanism, the galvanostatic charge−discharge curves of S0 and S6 for selected cycles at 0.1 C and CV profiles at a scanning rate of 0.3 mV s^{-1} are displayed in Figure 7. From Figure 7a,b, the initial charge capacity is 831.8 mAh/g for S0 and 1000.6 mAh/g for S6, far higher than the theoretical capacity of graphite (372 mAh/g), demonstrating that the sulfur-containing carbon materials could deliver significantly enhanced capacities. Meanwhile, an irreversible capacity loss of 522.3 mAh/g for S0 and 607.6 mAh/g for S6 occurring in the initial charge−discharge cycle could be ascribed to the decomposition of electrolyte and the formation of SEI films.[3,6,48,50] In the first discharge curve, an obvious plateau presents below 0.25 V for S0 and two plateaus at ∼1.7 and 0.4 V for S6. The absence of high-voltage plateau at ∼2.4 V (corresponding to elemental sulfur S_8 to Li ploysulfides) confirms that there is no residual S_8 in S6 after washing with the boiling CCl_4, and a similar result has also been reported in the literature.[32] The short plateau at ∼1.7 V presents in S6 and is invisible in S0, because other C−S bonds could form in S6 owing to the interaction of the sulfur added with the carbon yielded besides the C−S bonds in the thiophene-like structure, as evidenced by the TGA and Raman results. The corresponding CV profiles of S0 and S6 are shown in Figure 7c,d. Two prominent reduction peaks are present at ∼1.7 and 0.4 V in the first discharge process, and they are associated with the lithiation of the chemically bonded sulfur to Li_2S[32] and the formation of SEI films on the anode materials,[3,6,48,50] respectively. In the first anodic scan, S0 exhibits one small widened peak at ∼1.5−2.4 V (Figure 7c), owing to the overlap of the oxidation peaks related to the Li^+ extraction and Li_2S to Li polysulfide.[29,51,52] For S6 (Figure 7d), the obvious oxidation peak occurring at ∼2.4 V could be attributed to the conversion of Li_2S to Li polysulfide. In the subsequent cycles, the cathodic peak at 1.7 V and the anodic peak at 2.4 V become weaker and broader. These results are in good agreement with those obtained from the charge−discharge curves. For both S0 and S6, the profile in the first scan is different from those in the subsequent ones owing to the formation of SEI films and/or the loss of some irreversible lithium storage sites during the initial cathodic scan. However, the CV profiles almost overlap from the second cycle, suggesting the stable electrochemical performance of the sulfur-containing carbon materials.

To further understand the effect of the unique sulfur-containing 1D structure on rate performance, EIS spectra were measured for the charged cells of S0, S2, and S6 after cycling 50 times, as shown in Figure 8. The EIS reveal two depressed

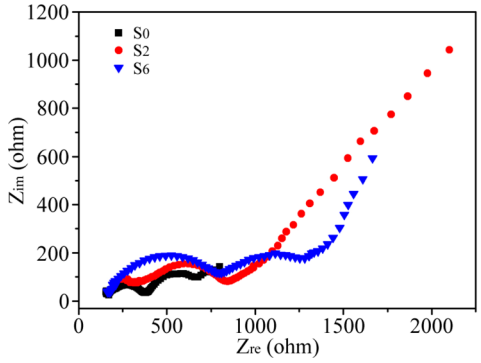

Figure 8. EIS of the charged cells of S0, S2, and S6 after cycling 50 times at 0.1 C.

semicircles in the high-to-medium frequency region, as well as an inclined line in the low-frequency region. The semicircles are associated, respectively, with the resistance of the SEI film formed on the electrode surface (R_{SEI}) and the charge-transfer resistance (R_{ct}), and the inclined line is associated with the Li-ion diffusion in the electrode, that is, the Warburg impedance (Z_W).[52,53] Obviously, the samples S2 and S6, which contain the unique carbon nanofibers, exhibit a larger slope than S0 (without the carbon nanofibers), indicative of the lower Li-ion diffusion impedance in S2 and S6 than in S0. Particularly, S6 possesses the largest line slope in the three samples because it is almost fully comprised of the carbon nanofibers with the graphene layers vertical to the axis direction. In other words, a faster Li-ion diffusion kinetics could be induced by these novel carbon nanofibers. Also from the EIS, the sum of R_{SEI} and R_{ct} for S0, S2, and S6 increases gradually, demonstrating the decreased electronic conductivity owing to the increased sulfur content. The larger total resistance of S6 than S2 results in the inferior rate performance of S6 at a high rate of 5.0 C, though the Z_w value of S6 is lower than that of S2. These results mean that both the ionic and electronic conductivities could influence the electrochemical performance of electrode materials, and they should match well to achieve increased comprehensive performance. For S6, the lower electronic conductivity is responsible for the lower capacity at the high rate of 5 C. The EIS results are in accordance with the rate performance displayed in Figure 6b.

4. CONCLUSIONS

In summary, we developed a novel method to simply synthesize carbon nanofibers with the graphene layers perpendicular to their length direction by the reaction between thiophene and sulfur at 550 °C in stainless steel autoclaves. The morphology of the products changes from the microspheres with no addition of other sulfur to the nanofibers with a molar ratio of 1:6 for thiophene to sulfur. The formation of nanofibers could

DOI: 10.1021/am508862e
ACS Appl. Mater. Interfaces 2015, 7, 5107−5115

be attributed to the promotion of sulfur on the morphology change in the presence of stainless steel as the catalyst. The graphene layers perpendicular to the axis direction could effectively shorten the diffusion path of Li ions in the nanofibers, and the high sulfur content contributes to the enhanced reversible capacity, so the sulfur-containing carbon nanofibers exhibiting excellent cycling performance and rate capabilities could be a potential anode material for LIBs with high performance.

■ ASSOCIATED CONTENT

Supporting Information

FESEM image of S0 and the corresponding elemental mappings of carbon and sulfur. EDX spectrum. TGA curves of S0 and S6 under nitrogen flow, elemental analysis data of S0, S2, and S6, TEM images of A0, A4, and A16. TEM images of the product obtained by the reaction of thiophene and sulfur with a molar ratio of 1:6 in a quartz tube placed in the autoclaves at 550 °C for 5 h. TEM images and electrochemical performance of the common carbon nanotubes with the graphene layers parallel to the length direction. TEM images of S6 after cycling 50 times. This material is available free of charge via the Internet at http://pubs.acs.org.

■ AUTHOR INFORMATION

Corresponding Authors

*Tel/Fax: +86 531 88392315. E-mail address: lunning66@sdu.edu.cn. (N.L.)

*E-mail: byj97@126.com (Y.-J.B.)

Notes

The authors declare no competing financial interest.

■ ACKNOWLEDGMENTS

This work was supported by Science and Technology Development Project of Shandong Province (2014GGX102009), the Independent Innovation Foundation of Shandong University, IIFSDU (2012ZD004), the National Natural Science Foundation of China (No. 51172131), Doctoral Foundation of Shandong Province (BS2013CL019), Science and Technology Development Project of Qingdao (13-1-4-186-jch), and Scientific Research Foundation of Shandong University of Science and Technology for Recruited Talents (2013RCJJ003).

■ REFERENCES

(1) Kim, C.; Yang, K. S.; Kojima, M.; Yoshida, K.; Kim, Y. J.; Kim, Y. A.; Endo, M. Fabrication of Electrospinning-Derived Carbon Nanofiber Webs for the Anode Material of Lithium-Ion Secondary Batteries. *Adv. Funct. Mater.* **2006**, *16*, 2393−2397.

(2) Chen, L.; Wang, Z. Y.; He, C. N.; Zhao, N. Q.; Shi, C. S.; Liu, E. Z.; Li, J. J. Porous Graphitic Carbon Nanosheets as a High-Rate Anode Material for Lithium-Ion Batteries. *ACS Appl. Mater. Interfaces* **2013**, *5*, 9537−9545.

(3) Li, X. F.; Liu, J.; Zhang, Y.; Li, Y. L.; Liu, H.; Meng, X. B.; Yang, J. L.; Geng, D. S.; Wang, D. N.; Li, R. Y.; Sun, X. L. High Concentration Nitrogen Doped Carbon Nanotube Anodes with Superior Li^+ Storage Performance for Lithium Rechargeable Battery Application. *J. Power Sources* **2012**, *197*, 238−245.

(4) Kawasaki, S.; Iwai, Y.; Hirose, M. Electrochemical Lithium Ion Storage Property of C60 Encapsulated Single-Walled Carbon Nanotubes. *Mater. Res. Bull.* **2009**, *44*, 415−417.

(5) Xiong, Z. L.; Yun, Y. S.; Jin, H. J. Applications of Carbon Nanotubes for Lithium Ion Battery Anodes. *Materials* **2013**, *6*, 1138−1158.

(6) Yoo, E. J.; Kim, J.; Hosono, E.; Zhou, H. S.; Kudo, T.; Honma, I. Large Reversible Li Storage of Graphene Nanosheet Families for Use in Rechargeable Lithium Ion Batteries. *Nano Lett.* **2008**, *8*, 2277−2282.

(7) Yang, S. B.; Huo, J. P.; Song, H. H.; Chen, X. H. A Comparative Study of Electrochemical Properties of Two Kinds of Carbon Nanotubes as Anode Materials for Lithium Ion Batteries. *Electrochim. Acta* **2008**, *53*, 2238−2244.

(8) Wang, X. X.; Wang, J. N.; Chang, H.; Zhang, Y. F. Preparation of Short Carbon Nanotubes and Application as an Electrode Material in Li-Ion Batteries. *Adv. Funct. Mater.* **2007**, *17*, 3613−3618.

(9) Wang, X. X.; Wang, J. N.; Su, L. F. Preparation and Electrochemical Performance of Ultra-Short Carbon Nanotubes. *J. Power Sources* **2009**, *186*, 194−200.

(10) Jian, K. Q.; Shim, H. S.; Schwartzman, A.; Crawford, G. P.; Hurt, R. H. Orthogonal Carbon Nanofibers by Template-Mediated Assembly of Discotic Mesophase Pitch. *Adv. Mater.* **2003**, *15*, 164−167.

(11) Mukhopadhyay, A.; Guo, F.; Tokranov, A.; Xiao, X. C.; Hurt, R. H.; Sheldon, B. W. Engineering of Graphene Layer Orientation to Attain High Rate Capability and Anisotropic Properties in Li-Ion Battery Electrodes. *Adv. Funct. Mater.* **2013**, *23*, 2397−2404.

(12) Chambers, A.; Park, C.; Baker, R. T. K.; Rodriguez, N. M. Hydrogen Storage in Graphite Nanofibers. *J. Phys. Chem. B* **1998**, *102*, 4253−4256.

(13) Laude, T.; Kuwahara, H.; Sato, K. $FeCl_2$-CVD Production of Carbon Fibres with Graphene Layers Nearly Perpendicular to Axis. *Chem. Phys. Lett.* **2007**, *434*, 78−81.

(14) Konno, H.; Sato, S.; Habazaki, H.; Inagaki, M. Formation of Platelet Structure Carbon Nanofilaments by a Template Method. *Carbon* **2004**, *42*, 2756−2759.

(15) Zhi, L. J.; Wu, J. S.; Li, J. X.; Kolb, U.; Müllen, K. Carbonization of Disclike Molecules in Porous Alumina Membranes: Toward Carbon Nanotubes with Controlled Graphene-Layer Orientation. *Angew. Chem.* **2005**, *117*, 2158−2161.

(16) Li, L. X.; An, B. G.; Nishihara, H.; Shiroya, T.; Aikyo, H.; Isojima, T.; Yamamoto, M.; Kyotani, T. Water-Dispersible Carbon Nanopods with Controllable Graphene Layer Orientation. *Chem. Commun.* **2009**, *30*, 4554−4556.

(17) Katsuki, H.; Matsunaga, K.; Egashira, M.; Kawasumi, S. Formation of Carbon Fibers from Naphthalene on Some Sulfur-Containing Substrates. *Carbon* **1981**, *19*, 148−150.

(18) Kim, M. S.; Rodríguez, N. M.; Baker, R. T. K. The Interplay Between Sulfur Adsorption and Carbon Deposition on Cobalt Catalysts. *J. Catal.* **1993**, *143*, 449−463.

(19) Tibbetts, G. G.; Bernardo, C. A.; Gorkiewicz, D. W.; Alig, R. L. Role of Sulfur in the Production of Carbon Fibers in the Vapor Phase. *Carbon* **1994**, *32*, 569−576.

(20) Ci, L. J.; Li, Y. H.; Wei, B. Q.; Liang, J.; Xu, C. L.; Wu, D. H. Preparation of Carbon Nanofibers by the Floating Catalyst Method. *Carbon* **2000**, *38*, 1933−1937.

(21) Romo-Herrera, J. M.; Cullen, D. A.; Cruz-Silva, E.; Ramírez, D.; Sumpter, B. G.; Meunier, V.; Terrones, H.; Smith, D. J.; Terrones, M. The Role of Sulfur in the Synthesis of Novel Carbon Morphologies: From Covalent Y-Junctions to Sea-Urchin-Like Structures. *Adv. Funct. Mater.* **2009**, *19*, 1193−1199.

(22) Tang, K.; Fu, L. J.; White, R. J.; Yu, L. H.; Titirici, M. M.; Antonietti, M.; Maier, J. Hollow Carbon Nanospheres with Superior Rate Capability for Sodium-Based Batteries. *Adv. Energy Mater.* **2012**, *2*, 873−877.

(23) Haerle, R.; Riedo, E.; Pasquarello, A.; Baldereschi, A. sp^2/sp^3 Hybridization Ratio in Amorphous Carbon from C1s Core-Level Shifts: X-ray Photoelectron Spectroscopy and First-Principles Calculation. *Phys. Rev. B* **2001**, *65*, 045101.

(24) Zhang, D. Y.; Hao, Y.; Zheng, L. W.; Ma, Y.; Feng, H. X.; Luo, H. M. Nitrogen and Sulfur Co-Doped Ordered Mesoporous Carbon with Enhanced Electrochemical Capacitance Performance. *J. Mater. Chem. A* **2013**, *1*, 7584−7591.

DOI: 10.1021/am508862e
ACS Appl. Mater. Interfaces 2015, 7, 5107−5115

(25) Poh, H. L.; Šimek, P.; Sofer, Z.; Pumera, M. Sulfur-Doped Graphene via Thermal Exfoliation of Graphite Oxide in H_2S, SO_2, or CS_2 Gas. *ACS Nano* **2013**, *7*, 5262−5272.
(26) Glenis, S.; Nelson, A. J.; Labes, M. M. Sulfur Doped Graphite Prepared via Arc Discharge of Carbon Rods in the Presence of Thiophene. *J. Appl. Phys.* **1999**, *86*, 4464−4466.
(27) Paraknowitsch, J. P.; Thomas, A.; Schmidt, J. Microporous Sulfur-Doped Carbon from Thienyl-Based Polymer Network Precursors. *Chem. Commun.* **2011**, *47*, 8283−8285.
(28) Ai, W.; Luo, Z. M.; Jiang, J.; Zhu, J. H.; Du, Z. Z.; Fan, Z. X.; Xie, L. H.; Zhang, H.; Huang, W.; Yu, T. Nitrogen and Sulfur Codoped Graphene: Multifunctional Electrode Materials for High-Performance Li-Ion Batteries and Oxygen Reduction Reaction. *Adv. Mater.* **2014**, *26*, 6186−6192.
(29) Zhang, Z. W.; Li, Z. Q.; Hao, F. B.; Wang, X. K.; Li, Q.; Qi, Y. X.; Fan, R. H.; Yin, L. W. 3D Interconnected Porous Carbon Aerogels as Sulfur Immobilizers for Sulfur Impregnation for Lithium−Sulfur Batteries with High Rate Capability and Cycling Stability. *Adv. Funct. Mater.* **2014**, *24*, 2500−2509.
(30) Chen, Y. M.; Li, X. Y.; Park, K. S.; Hong, J. H.; Song, J.; Zhou, L. M.; Mai, Y. W.; Huang, H. T.; Goodenough, J. B. Sulfur Encapsulated in Porous Hollow CNTs@CNFs for High-Performance Lithium−Sulfur Batteries. *J. Mater. Chem. A* **2014**, *2*, 10126−10130.
(31) Wu, Y. S.; Xu, C. M.; Guo, J. X.; Su, Q. M.; Du, G. H.; Zhang, J. Enhanced Electrochemical Performance by Wrapping Graphene on Carbon Nanotube/Sulfur Composites for Rechargeable Lithium−Sulfur Batteries. *Mater. Lett.* **2014**, *137*, 277−280.
(32) Zheng, S. Y.; Han, P.; Han, Z.; Zhang, H. J.; Tang, Z. H.; Yang, J. H. High Performance C/S Composite Cathodes with Conventional Carbonate-Based Electrolytes in Li−S Battery. *Sci. Rep.* **2014**, *4*, 4842.
(33) Zhang, L. S.; Li, W.; Cui, Z. M.; Song, W. G. Synthesis of Porous and Graphitic Carbon for Electrochemical Detection. *J. Phys. Chem. C* **2009**, *113*, 20594−20598.
(34) Huang, C.; Doong, R.; Gu, D.; Zhao, D. Y. Dual-Template Synthesis of Magnetically-Separable Hierarchically-Ordered Porous Carbons by Catalytic Graphitization. *Carbon* **2011**, *49*, 3055−3064.
(35) Zheng, M. T.; Zhang, H. R.; Xiao, Y.; Dong, H. W.; Liu, Y. L.; Xu, R. C.; Hu, Y. K.; Deng, B. Y.; Lei, B. F.; Liu, X. T. Large-Scale Synthesis and Enhanced Hydrogen Storage of Monodispersed Sulfur-Doped Carbon Microspheres by Hydro-Sulfur-Thermal Carbonization of Starch. *Mater. Lett.* **2013**, *109*, 279−282.
(36) Compagnini, G.; Puglisi, O.; Foti, G. Raman Spectra of Virgin and Damaged Graphite Edge Planes. *Carbon* **1997**, *35*, 1793−1797.
(37) Romo-Herrera, J. M.; Cullen, D. A.; Cruz-Silva, E.; Ramírez, D.; Sumpter, B. G.; Meunier, V.; Terrones, H.; Smith, D. J.; Terrones, M. The Role of Sulfur in the Synthesis of Novel Carbon Morphologies: From Covalent Y-Junctions to Sea-Urchin-Like Structures. *Adv. Funct. Mater.* **2009**, *19*, 1193−1199.
(38) Xiao, L. F.; Cao, Y. L.; Xiao, J.; Schwenzer, B.; Engelhard, M. H.; Saraf, L. V.; Nie, Z. M.; Exarhos, G. J.; Liu, J. A Soft Approach to Encapsulate Sulfur: Polyaniline Nanotubes for Lithium−Sulfur Batteries with Long Cycle Life. *Adv. Mater.* **2012**, *24*, 1176−1181.
(39) Li, X. L.; Cao, Y. L.; Qi, W.; Saraf, L. V.; Xiao, J.; Nie, Z. M.; Mietek, J.; Zhang, J. G.; Schwenzer, B.; Liu, J. Optimization of Mesoporous Carbon Structures for Lithium−Sulfur Battery Applications. *J. Mater. Chem.* **2011**, *21*, 16603−16610.
(40) Liang, C. D.; Dudney, N. J.; Howe, J. Y. Hierarchically Structured Sulfur/Carbon Nanocomposite Material for High-Energy Lithium Battery. *Chem. Mater.* **2009**, *21*, 4724−4730.
(41) Ji, L. W.; Rao, M. M.; Aloni, S.; Wang, L.; Cairns, E. J.; Zhang, Y. G. Porous Carbon Nanofiber−Sulfur Composite Electrodes for Lithium/Sulfur Cells. *Energy Environ. Sci.* **2011**, *4*, 5053−5059.
(42) Bulusheva, L. G.; Okotrub, A. V.; Kurenya, A. G.; Zhang, H. K.; Zhang, H. J.; Chen, X. H.; Song, H. H. Electrochemical Properties of Nitrogen-Doped Carbon Nanotube Anode in Li-Ion Batteries. *Carbon* **2011**, *49*, 4013−4023.
(43) Li, X. F.; Liu, J.; Zhang, Y.; Li, Y. L.; Liu, H.; Meng, X. B.; Yang, J. L.; Geng, D. S.; Wang, D. N.; Li, R. Y.; Sun, X. L. High Concentration Nitrogen Doped Carbon Nanotube Anodes with Superior Li^+ Storage Performance for Lithium Rechargeable Battery Application. *J. Power Sources* **2012**, *197*, 238−245.
(44) Wu, Y. Z.; Reddy, M. V.; Chowdari, B. V. R.; Ramakrishna, S. Long-Term Cycling Studies on Electrospun Carbon Nanofibers as Anode Material for Lithium Ion Batteries. *ACS Appl. Mater. Interfaces* **2013**, *5*, 12175−12184.
(45) Kumar, P. S.; Sahay, R.; Aravindan, V.; Sundaramurthy, J.; Ling, W. C.; Thavasi, V.; Mhaisalkar, S. G.; Madhavi, S.; Ramakrishna, S. Free-Standing Electrospun Carbon Nanofibres—A High Performance Anode Material for Lithium-Ion Batteries. *J. Phys. D: Appl. Phys.* **2012**, *45*, 265302.
(46) Ji, L. W.; Yao, Y. F.; Toprakci, O.; Lin, Z.; Liang, Y. Z.; Shi, Q.; Medford, A. J.; Millns, C. R.; Zhang, X. W. Fabrication of Carbon Nanofiber-Driven Electrodes from Electrospun Polyacrylonitrile/Polypyrrole Bicomponents for High-Performance Rechargeable Lithium-Ion Batteries. *J. Power Sources* **2010**, *195*, 2050−2056.
(47) Xiang, H. F.; Li, Z. D.; Xie, K.; Jiang, J. Z.; Chen, J. J.; Lian, P. C.; Wu, J. S.; Yu, Y.; Wang, H. H. Graphene Sheets as Anode Materials for Li-Ion Batteries: Preparation, Structure, Electrochemical Properties and Mechanism for Lithium Storage. *RSC Adv.* **2012**, *2*, 6792−6799.
(48) Chen, X. C.; Wei, W.; Lv, W.; Su, F. Y.; He, Y. B.; Li, B. H.; Kang, F. Y.; Yang, Q. H. A Graphene-Based Nanostructure with Expanded Ion Transport Channels for High Rate Li-Ion Batteries. *Chem. Commun.* **2012**, *48*, 5904−5906.
(49) Han, F. D.; Bai, Y. J.; Liu, R.; Yao, B.; Qi, Y. X.; Lun, N.; Zhang, J. X. Template-Free Synthesis of Interconnected Hollow Carbon Nanospheres for High-Performance Anode Material in Lithium-Ion Batteries. *Adv. Energy Mater.* **2011**, *1*, 798−801.
(50) Liu, F.; Song, S. Y.; Xue, D. F.; Zhang, H. J. Folded Structured Graphene Ppaper for High Performance Electrode Materials. *Adv. Mater.* **2012**, *24*, 1089−1094.
(51) Cao, Y. L.; Li, X. L.; Aksay, I. A.; Lemmon, J.; Nie, Z. M.; Yang, Z. G.; Liu, J. Sandwich-Type Functionalized Graphene Sheet−Sulfur Nanocomposite for Rechargeable Lithium Batteries. *Phys. Chem. Chem. Phys.* **2011**, *13*, 7660−7665.
(52) Swiderska-Mocek, A.; Rudnicka, E. Lithium−Sulphur Battery with Activated Carbon Cloth-Sulphur Cathode and Ionic Liquid as Electrolyte. *J. Power Sources* **2015**, *273*, 162−167.
(53) Kim, J.; Lee, D.; Jung, H.; Sun, Y.; Hassoun, J.; Scrosati, B. An Advanced Lithium−Sulfur Battery. *Adv. Funct. Mater.* **2013**, *23*, 1076−1080.

DOI: 10.1021/am508862e
ACS Appl. Mater. Interfaces 2015, 7, 5107−5115